Mechanical Systems and Signal Processing 169 (2022) 108625

Contents lists available at ScienceDirect

Mechanical Systems and Signal Processing

journal homepage: www.elsevier.com/locate/ymssp

Experimental measurement of track irregularities using a scaled track recording vehicle and Kalman filtering techniques

Sergio Muñoz [a,*], Pedro Urda [b], José L. Escalona [b]

[a] Department of Materials and Transportation Engineering, University of Seville, Spain
[b] Department of Mechanical and Manufacturing Engineering, University of Seville, Spain

ARTICLE INFO

Communicated by W.-X. Ren

Keywords:
Track surveying
Track recording vehicle
Kalman filter
Scaled track
Track irregularities
Experimental validation

ABSTRACT

The actual trend of railway industry on track surveying is heading up the development of fast automated methods for continuous monitoring of track quality. This paper presents a model-based methodology for the estimation of lateral and vertical track irregularities from different sensors mounted on a Track Recording Vehicle (TRV): an Inertial Measurement Unit (IMU), a gauge sensor and a position encoder. The proposed methodology, based on the Kalman filtering technique, allows a fast and accurate measurement of track irregularities, without the use of a total station (which usually makes the measurement process very slow). The proposed method has been validated through an experimental campaign carried out on a 90 m long 1:10, scaled track facility and a scaled TRV at the University of Seville. The use of the scaled TRV allows the measurement of the 90 metres long scaled track at an operation velocity of $V = 0.7$ m/s in only two minutes. The results of the estimation of track irregularities have been compared with a previous measurement of the mentioned scaled track using manual means, showing a good agreement: with errors lower than 0.7 mm in the short wavelength range D1, which is the most influential in the dynamic behaviour of the vehicle. Additionally, the obtained results have been analysed and compared in the different wavelength ranges, according to standards.

1. Introduction

As it is well known in the railway industry, vehicle dynamics is highly influenced by track irregularities. A track with a considerable degree of irregularity reduces the vehicle's comfort and, in extreme cases, can even jeopardize the passenger safety. According to the EN13848 Standard [1], acceptable limit levels for track irregularities are considered according to their wavelength in three different ranges: $D_1 = [3, 25]$ m, $D_2 = [25, 70]$ m and $D_3 = [70, 200]$ m. Therefore, in the evaluation of track geometry quality, irregularities should be analysed taking into account these wavelength ranges, as well as the maximum allowed forward velocity of a vehicle. Due to the need to ensure the quality level of track geometry, railway operators strive to keep their track infrastructures in the best possible conditions. This requires intensive maintenance work and, most importantly, regular monitoring of track conditions. Surveying a railroad track is a difficult and expensive task, forcing operators to invest a substantial part of their budget in surveying and maintaining the track regularly. Traditionally, the most extended ways to survey a track have been based on the use of the so-called measuring trolleys [2,3]. Normally, it is a device with a T-shape frame which can move along a track pushed by a human operator. These devices are instrumented with an encoder that registers the position of the trolley on the track, a distance sensor that measures the track gauge, a tilt sensor or inclinometer that measures the track cant angle and, in most cases, a prism whose relative position is determined by a total station. The combination of these sensors and the total station allows a

* Corresponding author.
E-mail address: sergiomunoz@us.es (S. Muñoz).

https://doi.org/10.1016/j.ymssp.2021.108625
Received 31 March 2021; Received in revised form 4 November 2021; Accepted 6 November 2021
Available online 25 November 2021

precise but slow measurement of the track and its irregularities. New generation devices also include Assisted Global Navigation Satellite System (AGNSS) for absolute positioning on the track with centimetre-level precision [4,5]. Despite their accuracy [6], the main handicap of a measuring trolley lies in its reduced measurement speed, between 100 to 200 metres per hour. In addition, vehicle traffic must be interrupted during the measurement process, which implies great costs for the operating company. The actual trend of track surveying methods moves towards the development of fully automated measuring procedures based on the dynamic response of the vehicle throughout the on-board monitoring of the track quality using Track Recording Vehicles (TRV) [7]. The use of automated on-board surveying systems not only allows fast and continuous monitoring of track conditions, but also avoids possible subjectivities in the measurements due to human intervention.

The theory behind any automated track surveying method is not trivial. Railway dynamics is governed by highly non-linear equations, making the estimation of track irregularities from the inertial response of the vehicle difficult, specially the calculation of lateral track irregularities. Different approaches for the calculation of track irregularities can be found in literature, an extended review is found in the work of [8,9]. In the work of Yang et al. [10] the authors use a time-dependent intrinsic correlation, unused to this day, to establish a relationship between the dynamic response of a vehicle and track irregularities with promising results. To do so, accelerations are decomposed in a series of intrinsic mode functions with different time scales. A similar approach is presented in Simian's work [11], where the authors find a correlation between the vehicle's acceleration and wheel-rail vertical irregularities using a frequency analysis. Real et al. [12] propose a procedure to obtain the vertical rail profile from the vertical acceleration by the use of the Fourier transform and transfer functions in the frequency domain. De Rosa et al. [13] present a frequency-domain based and two time-domain based methods to estimate the lateral and cross alignment based on vehicle dynamics measurements.

As an alternative, recent studies try to address railway irregularity measurement on the basis of machine learning and neural computing methods. Kraft et al. [14] have developed a black-box model of railway vehicles using neural networks for track geometry assessment. The use of black-box models trained with recurrent neural networks gives good results compared with multibody models for the assessment of lateral track irregularities. De Rosa et al. [15] have developed a method for the assessment of lateral track irregularities based on machine learning classification algorithms. The method has been developed using numerical simulations. Similarly, Tsunashima [16] has used machine learning classification and car-body sensors for track condition monitoring. This technique has been developed with the help of multibody simulations using the SIMPACK software and field tests.

However, the most commonly found methods in the literature for the estimation of track geometry and its irregularities are based on the use of Kalman filtering techniques. Kalman filters have traditionally been applied to other railway problems such as fault diagnosis in suspension systems [17,18], wheel rolling radius estimation [19] or adherence coefficient estimation [20] with success. In the work of Odashima et al. [21] vertical track irregularities are obtained by solving the inverse dynamics problem, using a Kalman filter as integrator and the car-body's measured acceleration. In the work of Lee et at. [22], a Kalman filter is used as a kind of integrator of lateral acceleration of the wheelset to obtain lateral displacements and, subsequently, a set of compensation filters are used in the corresponding wavelength bands to predict lateral irregularities. Along the same lines, it is the work of Wei et al. [23] that estimates track irregularities in urban lines using a Kalman filter to double integrate the vertical acceleration of the bogie frame. Xiao et al. in [24] propose a filter that estimates vertical track irregularities in railway bridges paying attention to the mechanical behaviour of such structures, very common in high-speed lines. A variation of the Extended Kalman Filter (EKF), the Extended Particle Filter (EPF) is used by Astikwa et al. in [25] to estimate vertical track irregularities using dynamic measurements. Kalman filtering techniques have also been integrated with innovative and quite sophisticated approaches as shown in the work of Jiang et al. [26] where track irregularities are obtained with a millimetre precision level using an instrumented manual trolley and a total station. In a similar way, Gao et al. use a Rauch–Tung–Striebel smoother multisensor fusion system to measure track irregularities in [27]. All these methods have the usage of acceleration and angular velocity measurements as estimation model inputs in common. However Weston et al. assure in [28] that track alignment can be determined by analysing standard deviation of the measured yaw angle exclusively. It must be noted that the majority of these works found in literature focus on the calculation of vertical track irregularities, while just a few of them deal with the estimation of lateral track irregularities due to its higher complexity.

The different methods described above represent different valid alternatives to obtain track irregularities from the measurements of an instrumented vehicle. Even though the use of artificial intelligence is gaining more visibility in the last years, there are a series of disadvantage in the use of this method. The main disadvantage is the need of a large enough set of data for the training process. These data are not always easy or even feasible to obtain, which results on a reduction of the precision of the estimated result. In addition, any slight change in the test conditions requires a new training process of the network. Despite of that, as it is shown in the literature, artificial intelligence methods are generally precise and computational efficient as long as the training process is performed correctly. The working principle of correlation methods is similar to artificial intelligence methods, with the difference that they do not require a training process. Finally, Kalman filter based method have the disadvantage that they need a kinematic or dynamic model that represents the performance of the vehicle. However, if the model is correctly parameterized, changes in the simulated vehicle can be easily introduced in the model. In addition, if they are correctly implemented, these methods can be computationally very efficient with real time capabilities. As a conclusion, the Kalman filter method can be considered as the most scientific of the three mentioned approaches and, if it is based on a reliable model, this method can offer a great performance.

The main goal of the present work is the development of an estimation procedure, based on the Kalman Filter technique, to measure the lateral and vertical track irregularities from different sensors mounted on a dedicated vehicle (Track Recording Vehicle). The proposed method, with the advantage of not needing a total station, allows a fast and accurate measurement of track irregularities. When comparing with previous works in literature, the proposed method obtains very good results in the estimation of both vertical and lateral track irregularities. Especially interesting are the results in the estimation of lateral track

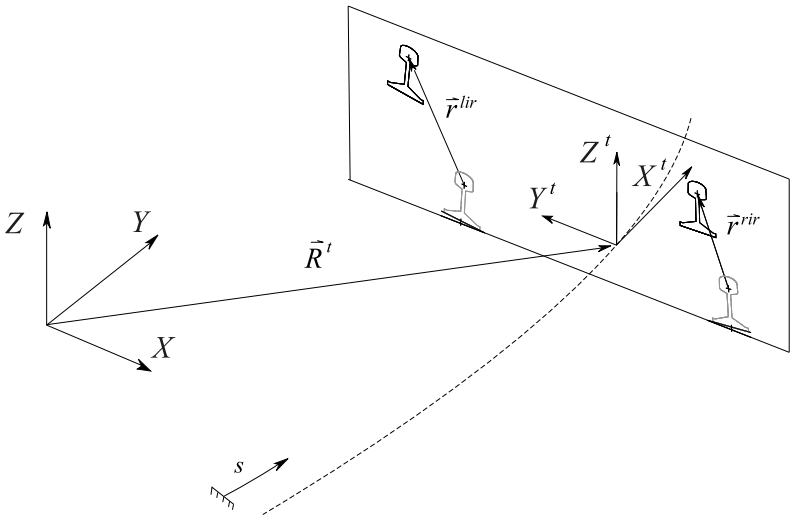

Fig. 1. Definition of track geometry.

irregularities, which are the most difficult type of irregularities to estimate and the most influential one in the dynamic behaviour of the vehicle. The proposed method has been tested with experimental data obtained with an scaled TRV running on a 5-inch gauge experimental track built at the School of Engineering of the University of Seville. As a main contribution, the presented method for the measurement of track irregularities is based exclusively on a kinematic multibody model of the vehicle, unlike other works found in literature that use more sophisticated dynamic models. Despite that, the obtained results demonstrate that the proposed method allows a precise way to obtain track irregularities. The estimated irregularities with the scaled TRV have been compared with a reference measurement obtained with a precise manual method. The obtained results in the estimation of track irregularities have been analysed in the space frequency domain, according to standards [1]. In this respect, even though there are three wavelength ranges considered in the standard (D1, D2 and D3), when evaluating the acceptable limits of track irregularities, the long wavelength range (D3) is not considered, since this range is not directly related with safety, but with vehicle rolling quality. Consequently, only the first two wavelength ranges (D1 and D2) will be considered in the present work.

This paper is organized as follows: Section 2 is devoted to the general definition of track irregularities. Section 3 presents the kinematic model of the TRV, while Section 4 explains the applied estimation technique in detail. Section 5 is devoted to the description of the experimental setup used. The obtained results and their comparison with the reference measurement are presented in Section 6. Summary and conclusions are found in Section 7.

2. Definition of track geometry

Track geometry is defined as the superposition of the design geometry and the irregularities, as it can be seen in Fig. 1.

The design geometry is defined by the track centre line and the cant angle. *Track frame* (TF) $\langle X^t, Y^t, Z^t \rangle$ is not a single frame but a field defined for each value of the arc-length coordinate along the horizontal projection of the track centre line, s. The absolute position vector of the TF with respect to inertial and *global frame* (GF) $\langle X, Y, Z \rangle$ is a function of arc-length s, as follows:

$$\mathbf{R}^t(s) = \begin{bmatrix} R_x^t(s) \\ R_y^t(s) \\ R_z^t(s) \end{bmatrix} \tag{1}$$

Orientation matrix $\mathbf{A}^t(s)$ of the TF with respect to the GF is defined through the Euler angles: yaw ψ^t (*heading* angle), pitch θ^t (vertical slope) and roll φ^t (*cant angle*). The yaw angle can have an arbitrary value but the roll and pitch are small angles. A small-angle approximation of orientation matrix $\mathbf{A}^t(s)$ is given by:

$$\mathbf{A}^t(s) \simeq \begin{bmatrix} \mathrm{c}\psi^t & -\mathrm{s}\psi^t & \varphi^t \mathrm{s}\psi^t + \theta^t \mathrm{c}\psi^t \\ \mathrm{s}\psi^t & \mathrm{c}\psi^t & \theta^t \mathrm{s}\psi^t - \varphi^t \mathrm{c}\psi^t \\ -\theta^t & \varphi^t & 1 \end{bmatrix} \tag{2}$$

Twist curvature ρ_{tw}, vertical curvature ρ_v and horizontal curvature ρ_h of the track are the space derivatives of roll angle φ^t, pitch angle θ^t yaw angle ψ^t with respect to the arc-length s, respectively.

As for irregularities, Fig. 1 shows the displacement of the rail heads due to irregularity in a cross-section of the track ($Y^t - Z^t$ plane). Irregularity vectors $\vec{r}^{lir}$ (*lir*, left rail irregularity) and $\vec{r}^{rir}$ (*rir*, right rail irregularity) describe the displacement of the rail

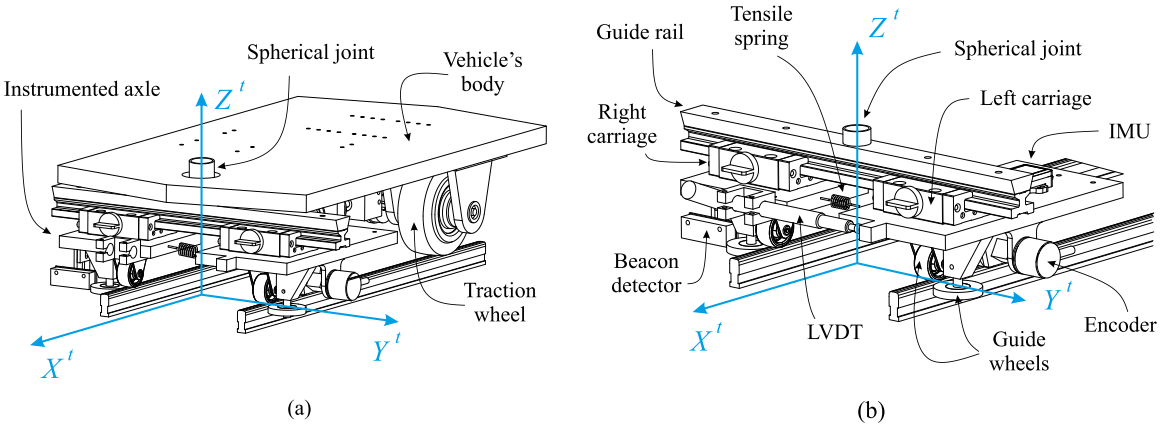

Fig. 2. (a) Track recording vehicle CAD. (b) Isolated instrumented axle CAD.

centre lines with respect to their design positions. The components of these vectors in the TF are functions of s, given by:

$$\bar{\mathbf{r}}^{lir} = \begin{bmatrix} 0 \\ y^{lir} \\ z^{lir} \end{bmatrix}, \quad \bar{\mathbf{r}}^{rir} = \begin{bmatrix} 0 \\ y^{rir} \\ z^{rir} \end{bmatrix} \tag{3}$$

The lateral and vertical irregularities of a track are usually defined by four well-known variables in the railway industry:

$$\begin{aligned} &\text{Alignment:} && \xi_{al} = \left(y^{lir} + y^{rir}\right)/2 \\ &\text{Vertical profile:} && \xi_{vp} = \left(z^{lir} + z^{rir}\right)/2 \\ &\text{Gauge variation:} && \xi_{gv} = y^{lir} - y^{rir} \\ &\text{Cross level:} && \xi_{cl} = z^{lir} - z^{rir} \end{aligned} \tag{4}$$

These irregularities can be divided into two different types: global irregularities as the variation of the track centre line (alignment and vertical profile), and relative irregularities as the variation of the relative position between both rails (gauge variation and cross-level).

3. Multibody model of the TRV

3.1. Description of the TRV

The vehicle is equivalent to a track trolley, but including an electric drive system. Fig. 2(a) shows the *Computational Assisted Design* (CAD) of the scaled Track Recording Vehicle. It is composed of two parts: the drive system, consisting of the vehicle's body and traction wheels, and the instrumented axle located in the front-end of the vehicle, which performs the measurements. Both parts are connected through a spherical joint that decouples the rotations of both bodies.

Fig. 2(b) shows the CAD of the instrumented axle. It includes two carriages which can slide along the guide rail. A couple of lateral guide wheels installed on both sides of the instrumented axle and a tensile spring that connects both carriages make it possible for the instrumented axle to perfectly follow the track geometry. During its operation, the left carriage where the IMU is installed is locked while the right one moves freely along the guide rail following the track irregularity. The linear variable differential transformer sensor (LVDT), that is attached to the right carriage (see Fig. 2(b)) measures the variation on the track gauge. The instrumented axle also includes a precision encoder that measures the travelled distance along the track and a beacon detector that register the position of a set of magnetic beacons distributed along the track and whose position was previously measured using a total station. Using the encoder and the position of the beacons the vehicle can be accurately located along the track.

Fig. 3 shows a simplified model of the kinematics of the instrumented axle.

This figure shows the *track frame* moving along the track centre line with forward velocity V and forward acceleration $\dot{V}$, and irregularity vectors $\vec{r}^{\,lir}$ and $\vec{r}^{\,rir}$ describing the displacement of the rail centre lines with respect to their design positions. The instrumented axle is assumed to comprise two bodies (left and right carriages in Fig. 2(b)) connected with a prismatic joint.

The following assumptions have been taken:

- The left body, which includes the installed IMU, is assumed to keep point Q in contact with the centre line of the left rail.
- The right body is assumed to keep point P in contact with the centre line of the right rail.
- The axle of the left body is perpendicular to the centre line of the left rail.

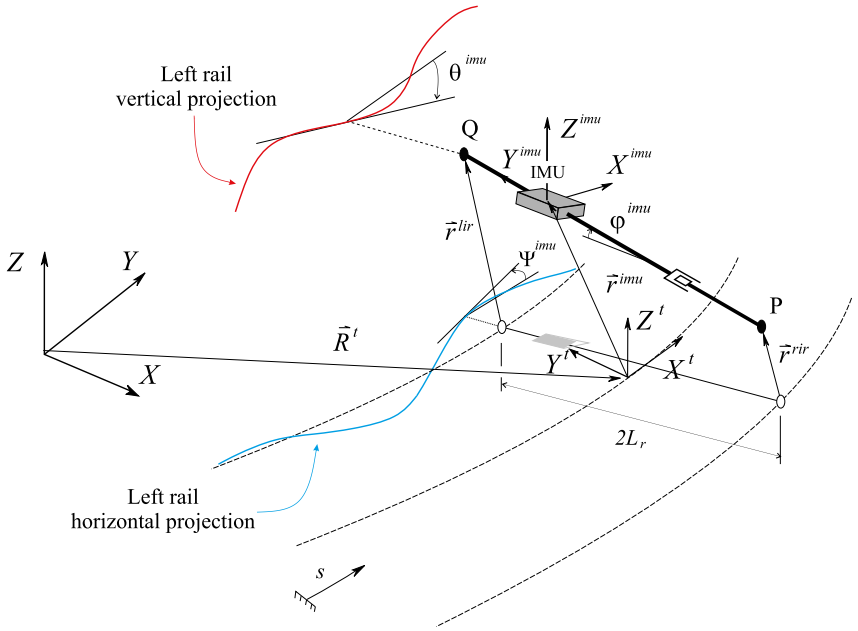

Fig. 3. Kinematics of the instrumented axle.

- The IMU is assumed to be installed in a vertical plane that contains points P and Q at distance d_y in the lateral direction and d_z in the vertical direction with respect to point Q.
- The three Euler angles that define the orientation of the IMU with respect to the TF (φ^{imu}, θ^{imu} and ψ^{imu}) are supposed to be small.

The first two assumptions are reasonable due to the mechanical design of the instrumented axle. The spring that connects the two main bodies of the instrumented axle and the horizontal and vertical wheels attached to them that roll over the rails guarantee that there exist two non-material points P and Q that fulfil these kinematic constraints. As regards the third assumption, since the left and right rail threads are not parallel, the instrumented axle cannot be perpendicular to both lines simultaneously, but the relative angle of the axle with respect to the perpendicular line is very small. Therefore, the assumption of perpendicularity of the left body is somehow arbitrary (the right body could be selected as perpendicular) but the resulting inaccuracies are very small. The fourth assumption is not true. However, it is well known from rigid body kinematics that in a rigid body that does not rotate, the acceleration of all points is the same. If the body rotates, the difference in acceleration between two points is proportional to their relative distance. Because the distance between the IMU and the line that connects P and Q is also small, the measurement of the IMU can be considered accurate. Anyway, the inaccuracy due to this assumption can be corrected if the angular velocity and acceleration of the axle are known. However, in this paper we have consider that this correction is not needed for the sake of simplicity of the resulting equations. In the last assumption, the angles that are assumed to be small are the relative angles of the IMU with respect to the TF. It must be note that the absolute angles of the track or the absolute angles of the IMU may become large in curved tracks, but the relative angles remain small even with small radius of curvature of the track.

Using the kinematics of an irregular track shown in Fig. 3 and the simplifying assumptions stated above, the following relationships can be established:

$$\begin{aligned} r_y^{imu} &= y^{lir} + L_r - d_y \\ r_z^{imu} &= z^{lir} + d_z \\ \varphi^{imu} &= (z^{lir} - z^{rir})/2L_r \\ \theta^{imu} &= -\frac{dz^{lir}}{ds} = -z^{lir\prime} \\ \psi^{imu} &= \frac{dy^{lir}}{ds} = y^{lir\prime} \\ d_{PQ} &= 2L_r + y^{lir} - y^{rir} \end{aligned} \tag{5}$$

where r_y^{imu} and r_z^{imu} are the non-zero components of the position vector of the IMU with respect to the TF, and $2L_r$ is the nominal gauge (distance between both rails without irregularities). For the fourth and fifth expressions in Eq. (5), it assumed that local axis X^{imu} is tangent to the 3D curve of the left rail at all instants (see left rail lateral and vertical projections shown in Fig. 3). For the last expression, the distance between points P and Q, is assumed to be equal to its horizontal projection.

Finally, by time-derivation of Eq. (5), the following expressions can be obtained, which will be useful later:

$$\begin{aligned}
\dot{r}_y^{imu} &= \dot{V} y^{lir\prime} + V^2 y^{lir\prime\prime} \\
\dot{r}_z^{imu} &= \dot{V} z^{lir\prime} + V^2 z^{lir\prime\prime} \\
\dot{\varphi}^{imu} &= V(z^{lir\prime} - z^{rir\prime})/2L_r \\
\dot{\theta}^{imu} &= -V z^{lir\prime\prime} \\
\dot{\psi}^{imu} &= V y^{lir\prime\prime}
\end{aligned} \tag{6}$$

It is important to note that, although the IMU's trajectory follows more closely the left rail irregularity, the assumed kinematic model accounts for the effect of the 3D geometry of the left and the right irregular rails. Therefore, there is no reason to assume that the lack of symmetry of the instrumented axle can induce measurements more related to the left rail irregularities.

3.2. Kinematics of the IMU

For the kinematic description of the left body, to which the IMU is attached, the following coordinates are used:

$$\mathbf{q}^{imu} = \begin{bmatrix} s^{imu} & r_y^{imu} & r_z^{imu} & \varphi^{imu} & \theta^{imu} & \psi^{imu} \end{bmatrix}^T \tag{7}$$

where s^{imu} is the arc length of the track frame that follows the body motion, $\bar{\mathbf{r}}^i = \begin{bmatrix} 0 & r_y^i & r_z^i \end{bmatrix}^T$ is the local position vector of the IMU frame with respect to the TF resolved in the TF, and φ^{imu}, θ^{imu} and ψ^{imu} are the three Euler angles that define the orientation of the IMU with respect to the TF. Assuming that the three Euler angles are small, the following kinematic linearization of the IMU to the TF rotation matrix is obtained:

$$\mathbf{A}^{t,imu} \simeq \begin{bmatrix} 1 & -\psi^{imu} & \theta^{imu} \\ \psi^{imu} & 1 & -\varphi^{imu} \\ -\theta^{imu} & \varphi^{imu} & 1 \end{bmatrix} \tag{8}$$

The absolute acceleration of the IMU frame, projected in the TF, is given by [29]:

$$\bar{\ddot{\mathbf{R}}}^{imu} = \bar{\ddot{\mathbf{R}}}^t + \bar{\ddot{\mathbf{r}}}^{imu} + \left(\tilde{\bar{\boldsymbol{\alpha}}}^t + \tilde{\bar{\boldsymbol{\omega}}}^t \tilde{\bar{\boldsymbol{\omega}}}^t\right) \bar{\mathbf{r}}^{imu} + 2\tilde{\bar{\boldsymbol{\omega}}}^t \bar{\dot{\mathbf{r}}}^{imu} \tag{9}$$

And the absolute angular velocity of the IMU frame resolved in the IMU frame, under the small-angles assumption, is given by [29]:

$$\hat{\boldsymbol{\omega}}^{imu} = \hat{\boldsymbol{\omega}}^t + \hat{\boldsymbol{\omega}}^{t,imu} = \left(\mathbf{A}^{t,imu}\right)^T \bar{\boldsymbol{\omega}}^t + \hat{\boldsymbol{\omega}}^{t,imu} \tag{10}$$

As it can be found in [29], the terms associated with the TF are given by:

$$\bar{\ddot{\mathbf{R}}}^t = \begin{bmatrix} \dot{V} \\ \rho_h V^2 \\ -\rho_v V^2 \end{bmatrix}, \quad \bar{\boldsymbol{\omega}}^t = \begin{bmatrix} \rho_{tw} V \\ \rho_v V \\ \rho_h V \end{bmatrix}, \quad \bar{\boldsymbol{\alpha}}^t = \begin{bmatrix} \rho_{tw} \dot{V} \\ \rho_v \dot{V} \\ \rho_h \dot{V} + \rho'_h V^2 \end{bmatrix} \tag{11}$$

3.3. IMU signals

The IMU has a 3D gyroscope and a 3D accelerometer. The 3D accelerometer signals include the three components of the absolute acceleration in the IMU frame, plus the three components of the gravity vector, which is assumed to act in the absolute Z direction:

$$\mathbf{a}^{acm} = \left(\mathbf{A}^{t,imu}\right)^T \bar{\ddot{\mathbf{R}}}^{imu} + \left(\mathbf{A}^t \mathbf{A}^{t,imu}\right)^T \begin{bmatrix} 0 & 0 & g \end{bmatrix}^T \tag{12}$$

where $\mathbf{a}^{acm}$ is an array that includes the quantities measured by the 3D accelerometer.

The 3D gyroscope provides three digital signals that measure the three components of the IMU absolute angular velocity in the body frame, as follows:

$$\boldsymbol{\omega}^{gyr} = \hat{\boldsymbol{\omega}}^{imu} \tag{13}$$

where $\boldsymbol{\omega}^{gyr}$ is an array that includes the quantities measured by the 3D gyroscope.

3.4. Simplifying assumptions

In order to simplify previous equations, the following assumptions have been taken:

- The pitch and roll angles of the TF with respect to the GF are considered null ($\theta^t = \varphi^t = 0$), which leads to: $\rho_v = \rho_{tv} = 0$. This is common practice in the railway field, which considers that the design geometry has neither a vertical slope nor a cant angle. In this case, both the real vertical slope and the real cant angle are included as a part of the irregularities.
- The relative displacement of the IMU frame with respect to the TF is small, so it can be assumed that the relative centripetal and Coriolis acceleration are negligible in comparison with the second derivatives of $\bar{\mathbf{r}}^{imu}$. This assumption is equivalent to eliminating the third and fourth terms of the right-hand side of Eq. (9).

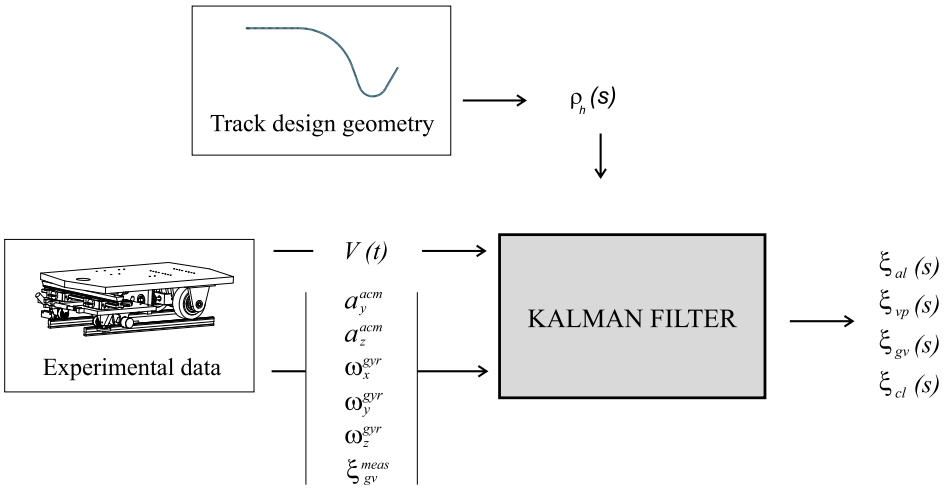

Fig. 4. Estimation procedure.

- The relative orientation of the IMU with respect to the TF is so small that the components of the absolute angular velocity of the TF are the same when projected to the TF or when projected to the IMU frame. This assumption is equivalent to making $\mathbf{A}^{t,imu}$ equal to the identity matrix in Eq. (10).

As demonstrated in [29], and taking into account the simplifying assumptions, the signal obtained from the accelerometer and the gyroscope presented in Eqs. (12) and (13) can be written as:

$$\begin{bmatrix} a_y^{acm} \\ a_z^{acm} \end{bmatrix} = \begin{bmatrix} \dot{r}_y^{imu} + g\varphi^{imu} + \rho_h V^2 \\ \dot{r}_z^{imu} + g \end{bmatrix} \tag{14}$$

$$\begin{bmatrix} \omega_x^{gyr} \\ \omega_y^{gyr} \\ \omega_z^{gyr} \end{bmatrix} = \begin{bmatrix} \dot{\varphi}^{imu} \\ \dot{\theta}^{imu} \\ \dot{\psi}^{imu} + \rho_h V \end{bmatrix} \tag{15}$$

Additionally, the equation related to the gauge variation must be included in the measurements of the Kalman filter, as it will described in the next section:

$$\xi_{gv}^{meas} = d_{PQ} - 2L_r = y^{lir} - y^{rir} \tag{16}$$

where the nominal gauge ($2L_r$) has been subtracted from the distance between points P and Q measured by the LVDT sensor (last expression of Eq. (5)).

4. Irregularity estimation technique

The main objective of this work is to estimate the lateral and vertical irregularities of a track from the measurements from the different sensors mounted on the TRV. To this end, a model-based numeric procedure based on Kalman filtering techniques has been used. As commented, the estimation technique is based on the kinematic model of the front mechanism of the vehicle, presented in Section 3. The estimation technique, which is graphically summarized in Fig. 4, is explained next.

As it can be observed, the estimation procedure is based on a Kalman filter, whose design will be explained later. The filter has two different kind of inputs. On one hand, the curvature of the ideal track centre line (ρ_h) as a function of arc-length coordinate s. Notice that the definition of the track centre line is needed in the estimation technique to calculate the accelerations and angular velocities measured by the IMU, which are due to the movement of the TF with respect to the GF. On the other hand, the Kalman filter needs the experimental data of the dynamic response of the mechanism as inputs: the vehicle forward velocity (V), measurements from the accelerometer (a_y^{acm} and a_z^{acm}) and from the gyroscope (ω_x^{gyr}, ω_y^{gyr} and ω_z^{gyr}), and gauge variation (ξ_{gv}^{meas}). All these data are acquired from one encoder and an inertial sensor unit (IMU) installed in the vehicle, and synchronized through a data acquisition system, at the same sampling rate (250 Hz in the present work). From all these data inputs, and making use of the Kalman filter, the four track irregularities can be estimated.

4.1. Design of the Kalman filter

As previously explained, the estimation technique is based on the well-known Kalman filter algorithm [30], which is briefly defined as follows. The state vector includes the lateral and vertical displacement of both rails with respect to their ideal position, and their first and second spatial derivatives, as:

$$\mathbf{x} = \begin{bmatrix} y^{lir} & y^{rir} & y^{lir\prime} & y^{rir\prime} & y^{lir\prime\prime} & y^{rir\prime\prime} & z^{lir} & z^{rir} & z^{lir\prime} & z^{rir\prime} & z^{lir\prime\prime} & z^{rir\prime\prime} \end{bmatrix}^T \tag{17}$$

The measurement vector includes accelerometer and gyroscope signals measured by the IMU, and the gauge variation measured by the LVDT distance sensor, plus two additional measurements of the lateral and vertical displacement of the left rail:

$$\mathbf{z}_{meas} = \begin{bmatrix} a_y^{acm} & a_z^{acm} & \omega_x^{gyr} & \omega_y^{gyr} & \omega_z^{gyr} & \xi_{gv}^{meas} & r_y^{imu} & r_z^{imu} \end{bmatrix}^T \tag{18}$$

Most of the components of this measurement vector are directly obtained from the IMU mounted on the vehicle. However, the measurement of the lateral and vertical displacement of the left rail, r_y^{imu} and r_z^{imu}, are not real measurements but virtual sensors, which in practice always provide constant values. The inclusion of virtual sensors in the measurement vector has been shown to offer an improvement in the performance of the Kalman filter in previous works [31]. It has two purposes. On one hand, it makes the system observable. On the other hand, from the practical point of view, the virtual sensor avoids a drift in the prediction of lateral and vertical irregularities. The inclusion of a virtual sensors with constant measurements can be seen as a highly disturbing procedure. To avoid this, it is very important an adequate selection of the variance associated with the Gaussian error of these virtual sensors, which must be carefully chosen to avoid the drift while keeping a good accuracy. If the value of the covariance is high, the virtual sensors have little influence in the results, being weak their effect on eliminating the drift. On the other hand, if the value of the covariance is small, the effect of the virtual sensor is strong, flattening the curve of the estimated irregularities. Consequently, the covariance of the noise associated with the virtual sensors must coincide with the covariance of the expected irregularities. This solution has been proven to give good results in previous works [31]

The equation of the Kalman filter in a discrete form can be expressed as follows:

$$\mathbf{x}_k = \mathbf{F}\, x_{k-1} + \mathbf{v}_k \tag{19}$$

where subscript k represents discrete time, and $\mathbf{F}$ is the state transition matrix, which can be obtained as:

$$\mathbf{F} = \begin{bmatrix} \mathbf{F}_L & 0 \\ 0 & \mathbf{F}_V \end{bmatrix}; \qquad \mathbf{F}_L = \mathbf{F}_V = \begin{bmatrix} 1 & 0 & V\Delta t & 0 & 0 & 0 \\ 0 & 1 & 0 & V\Delta t & 0 & 0 \\ 0 & 0 & 1 & 0 & V\Delta t & 0 \\ 0 & 0 & 0 & 1 & 0 & V\Delta t \\ 0 & 0 & 0 & 0 & 1 & 0 \\ 0 & 0 & 0 & 0 & 0 & 1 \end{bmatrix} \tag{20}$$

Notice that the system model is just an integrator and state transition matrix $\mathbf{F}$ depends on the forward velocity, V, and the time increment, Δt. In this case, term $\mathbf{v}_k$ is the process noise, which can be modelled as a zero-mean Gaussian noise with covariance matrix $\mathbf{Q}$.

The measurement process can be expressed through the following equation:

$$\mathbf{z}_k = \mathbf{H}\mathbf{x}_k + \mathbf{G} + \mathbf{w}_k \tag{21}$$

where subscript k represents discrete time, $\mathbf{H}$ is the measurement transition matrix and $\mathbf{G}$ is an input matrix. These matrices can be obtained by substituting Eqs. (5)–(6) for Eqs. (14)–(16), obtaining:

$$H = \begin{bmatrix} 0 & 0 & \dot{V} & 0 & V^2 & 0 & g/2L_r & -g/2L_r & 0 & 0 & 0 & 0 \\ 0 & 0 & 0 & 0 & 0 & 0 & 0 & 0 & \dot{V} & 0 & V^2 & 0 \\ 0 & 0 & 0 & 0 & 0 & 0 & 0 & 0 & V/2L_r & -V/2L_r & 0 & 0 \\ 0 & 0 & 0 & 0 & 0 & 0 & 0 & 0 & 0 & 0 & -V & 0 \\ 0 & 0 & 0 & 0 & V & 0 & 0 & 0 & 0 & 0 & 0 & 0 \\ 1 & -1 & 0 & 0 & 0 & 0 & 0 & 0 & 0 & 0 & 0 & 0 \\ 1 & 0 & 0 & 0 & 0 & 0 & 0 & 0 & 0 & 0 & 0 & 0 \\ 0 & 0 & 0 & 0 & 0 & 0 & 1 & 0 & 0 & 0 & 0 & 0 \end{bmatrix} \tag{22}$$

$$\mathbf{G} = \begin{bmatrix} \rho_h V^2 , & g , & 0 , & 0 , & \rho_h V , & 0 , & (L_r - d_y) , & d_z \end{bmatrix}^T \tag{23}$$

In this case, term $\mathbf{w}_k$ is the measurement noise, which can be modelled as a zero-mean Gaussian noise with covariance matrix $\mathbf{R}$.

5. Experimental setup

This section is devoted to the experimental setup that has been used to experimentally validate the proposed estimation algorithm, main contribution of this work. Firstly, the main features of the experimental scaled track are presented and, secondly, the final assembly of the scaled TRV and its instrumentation are also explained in detail.

Additionally, the methodology proposed in the present work has been compared with an alternative methodology previously presented by the authors [32], which also makes use of the same TRV but with a different configuration.

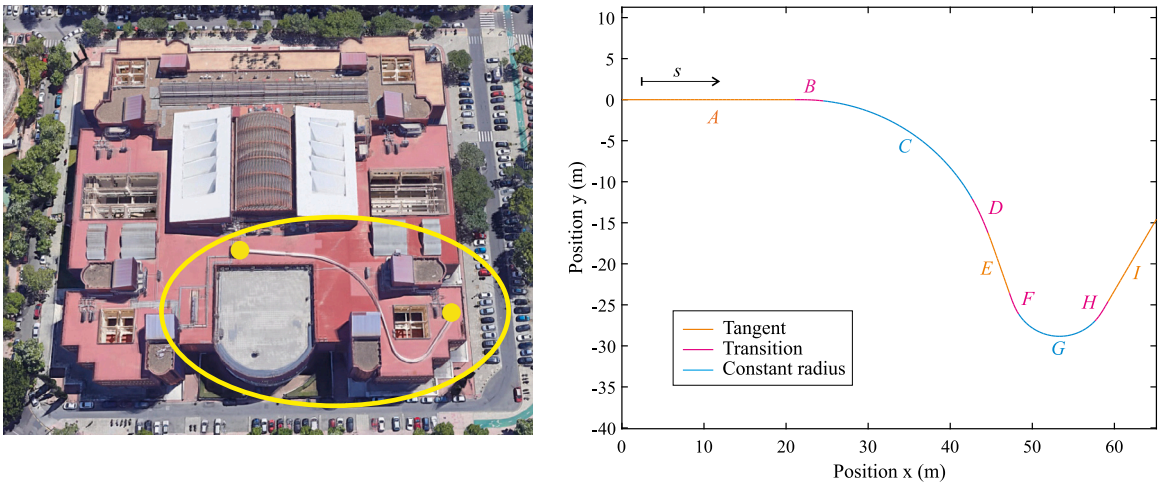

Fig. 5. (a) Aerial view of the scaled track. (b) Plan view of the scaled track.

Fig. 6. (a) Scaled track and metallic benches. (b) Adjustable mechanisms.

5.1. Experimental scaled track

This unique facility is located on the rooftop of the School of Engineering at the University of Seville as it is shown in Fig. 5(a). It is a 90-m long 5-inch-wide scaled track whose design geometry consists of a combination of tangent sections, transitions and constant curvature sections, like any other railway track. The different track segments of this particular track are depicted in Fig. 5(b), where different types of section have been highlighted in different colours. The lengths of the different track segments are summarized in Table 1.

The rails have been machined in three metre long pieces of AISI-304 stainless steel, reproducing a scaled version of an UIC-54 standard profile. The different sections are not welded with each other, but they are mechanically linked using special pieces. Both rails fit in a series of mechanisms that simulate a real track sleeper. The mechanisms are rigidly attached to a set of metallic benches leaning on the ground (see Fig. 6(a)). These benches were precisely located and levelled using a total station before the rails were installed. The mechanisms that support the rails give a unique value to the scaled track: they have been designed to allow the manual introduction of track irregularities (see Fig. 6(b)). With the correct actions on each mechanism, track gauge, cant angle and relative height between both rails can be modified precisely. The cant angle in the different curve sections has been changed manually in order to cancel the centrifugal force effects of a potential vehicle that moves along the track at a forward speed of 1.5 m/s. Taking into account that the scaled reduction of this velocity corresponds to 15 m/s on a full scaled track, which is an average maximum velocity for many metropolitan trains.

Table 1
Ideal geometry of the experimental scaled track.

Section	Length	Section type
A	22 m	Tangent
B	3 m	Transition
C	26 m	Constant radius
D	3 m	Transition
E	6 m	Tangent
F	3 m	Transition
G	12 m	Constant radius
H	3 m	Transition
I	12 m	Tangent

Table 2
List of sensors installed in the TRV for each methodology.

TRV + KF method	TRV + TS method
Encoder	Encoder
LVDT	LVDT
IMU	Inclinometer
	Total station

After installation, the scaled track geometry was measured using an accurate, but slow and tedious, manual method: the track centre line was measured by using a total station, while the track gauge and cant angle were obtained using a gauge sensor and an inclinometer. These three measurements are enough to determine the actual geometry of the scaled track and its four irregularities: alignment, vertical profile, gauge variation and cross-level. The measurement of the track centre line and its associated irregularities using manual methods are considered as the reference data that will be compared with the irregularity estimation, using the TRV, in a next section.

5.2. Design and instrumentation of the TRV

As previously commented, the proposed methodology has been compared with an alternative methodology previously presented by the authors [32]. For both methodologies, the same TRV has been used, but with different configurations (see Table 2). Both methods are explained as follows:

- *Track Recording Vehicle with Kalman Filter* (TRV + KF).
  This is the methodology proposed in the present work, which is based on the Kalman Filtering techniques. The sensors to be installed in the TRV are: an encoder, an LVDT distance sensor and an IMU.
- Track Recording Vehicle with Total Station (TRV + TS).
  This alternative methodology, presented by the authors in a previous work, is based on the use of a total station. The sensors to be installed in the TRV are: an encoder to measure the travelled distance, an LVDT distance sensor to measure the gauge variation and the total station together with a reflector installed in the TRV to obtain the geometry of the track centre line. The details of this methodology can be found in [32].

With the previous alternative methodology (TRV + TS), very good results in the measurement of track irregularities were obtained, reducing the time required to measure a track significantly when compared with a manual method. However, the maximum accuracy of the total station (0.2 mm) is only achievable if the total station and the target installed in the TRV are separated by less than 20 m. For this reason, due to the large dimension of the scaled track (90 m) and in order to guarantee maximum precision in the measurement with the total station, the track was measured in three sections, requiring subsequent post-processing.

With the new methodology proposed in this work (TRV + KF), based on the data from the IMU together with the Kalman Filter, the use of the total station can be avoided. In this way, the geometry of the entire length of the track can be measured at once, avoiding subsequent post-processing and reducing the measurement time as much as possible.

Fig. 7(a) shows the final assembly of the Track Recording Vehicle, equipped with sensors and all the instrumentation. The configuration presented in the figure includes all sensors, thus being valid for both methodologies under study: (TRV + KF) and (TRV + TS).

The vehicle is powered by a brushless motor that is connected to a differential mechanism that actuates both traction wheels. The differential mechanism guarantees that the traction wheels will not derail even though they are not conical. To control the vehicle and acquire the sensors measurements, the vehicle is equipped with a NI-MyRIO Real Time (RT) computer. The acquisition software and control have been entirely programmed using Labview. For clarity reasons, the instrumented axle is presented in Fig. 7(b), isolated on the track.

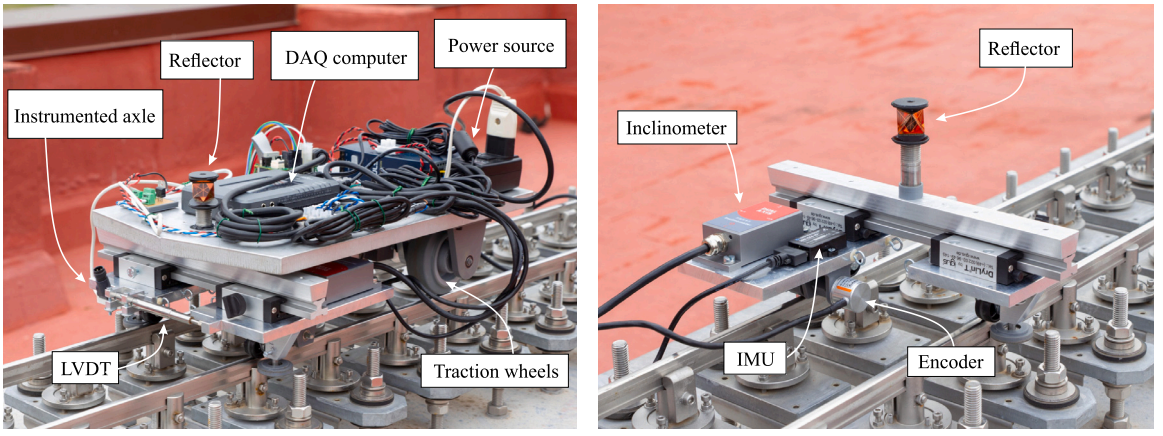

Fig. 7. TRV on the scaled track.

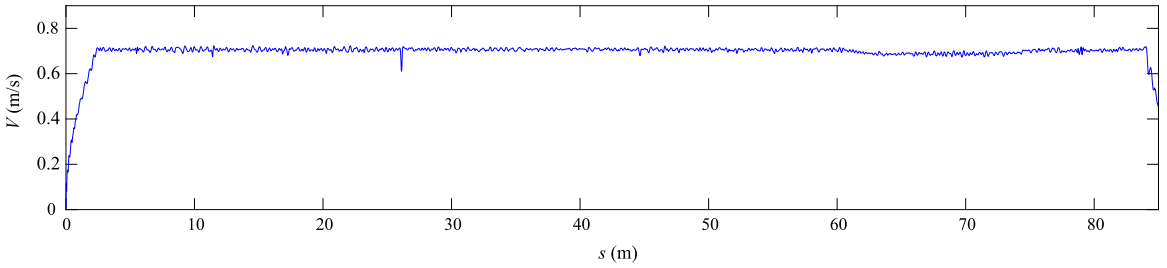

Fig. 8. Forward velocity profile.

6. Results and comparison

In this section, the proposed estimation technique is validated and its performance analysed. To do so, a complete campaign of six experiments has been carried out, involving different conditions: three different forward velocity levels (0.5 m/s, 0.7 m/s and 0.9 m/s). In the present work, only one of the experiments will be presented as representative: the vehicle moving forward on the track at a constant velocity of $V = 0.7$ m/s, for a total length of 85 m. The experiment with intermediate forward velocity level has been chosen as representative. However, it must be pointed out that similar results in the estimation of track irregularities have been obtained for the rest of the experiments.

The Kalman filter needs an estimation of the sensor noise variance for the prior calculation of the covariance matrices, **Q** and **R**. The noise variance has been estimated from the data sheet of the inertial measurement units. Therefore, the following values have been taken for the different sensors: a value of $(0.005)^2$ m^2/s^4 for the accelerometers (a_y^{acm} and a_z^{acm}), a value of $(0.0005)^2$ rad^2/s^2 for the gyroscopes (ω_x^{gyr}, ω_y^{gyr} and ω_z^{gyr}), and a value of $(0.0001)^2$ m^2 for the LVDT distance sensor (ξ_{gv}^{meas}). For the lateral and vertical displacement (r_y^{imu} and r_z^{imu}), a value of 5^2 mm^2 has been set, which is the order of expected value of the irregularities.

6.1. Input data from measurements

In this section, the input data from the experiment under study ($V = 0.7$ m/s) are presented. Firstly, the forward velocity profile obtained from the encoder installed in the vehicle is presented in Fig. 8. As observed, the forward velocity experiences an initially steep increasing slope until reaching the set-point value, when oscillations are observed before the stabilization. Similar behaviour is observed at the end of the ride, when the vehicle brakes.

Secondly, the experimental data from the inertial sensors installed in the vehicle are presented in Figs. 9 and 10, for the sensors related to lateral and vertical motion, respectively.

It must be note that some peaks distributed through the experiment can be observed in sensor data related to vertical motion, Fig. 10. Those peaks are due to the small gap between each two consecutive rail sections. Those gaps were intentionally introduced during the track assembly process in order to compensate for the effects of temperature.

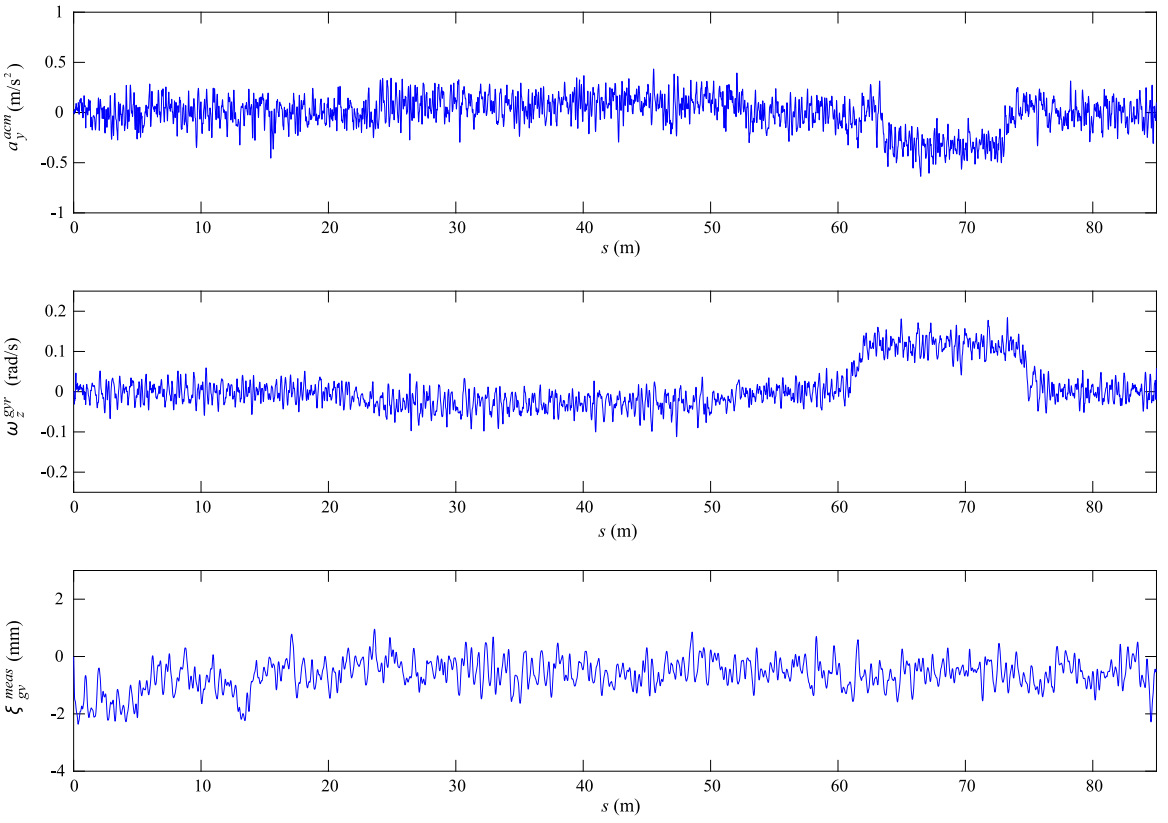

Fig. 9. Sensor data related to lateral motion.

6.2. Estimation of track irregularities

Once the track centre line geometry and its irregularities have been measured by manual methods, to be used as reference values, the prediction of the lateral and vertical irregularities has been carried out through the proposed Kalman filter algorithm. To this end, the experimental data acquired during the experiment under study, presented in Section 6.1, have been used as inputs.

The results of the estimation of track irregularities obtained with the proposed method (TRV + KF) are presented next, compared with the reference irregularities. Additionally, the results obtained by the alternative method previously presented by the authors (TRV + TS) have also been included in the comparison. Fig. 11 shows the estimation of track irregularities for the whole track length, by both methods under study. It should be noted that the three profiles presented in Fig. 11, estimations and reference, have been filtered with a Butterworth bandpass filter in the range of interest according to standards [1]: frequencies corresponding to a wavelength range between 0.3 and 7 m for the 1:10 scaled track (D1–D2 range). Note that, the D1–D2 range for a real scale track (λ = 3–70 m) corresponds to (λ = 0.3–7 m) in a 1:10 scaled track.

For a more in-depth analysis, the results of the estimation are presented separately in each wavelength range: D1 range (λ = 0.3–2.5 m) in Fig. 12 and D2 range (λ = 2.5–7 m) in Fig. 13. Note that, to better analyse the graphical results, the transition segments have been highlighted in Figs. 11–13.

In order to numerically evaluate the results achieved with the proposed Kalman filter estimator, an accuracy index has been calculated:

$$J = rms\,(\xi_{est} - \xi_{real}) \tag{24}$$

This is an absolute accuracy index, calculated as the root mean square value (rms) of the difference between the estimated and real irregularity. This index J has length units and is particularly useful and intuitive for measuring the disagreement of the estimation with the real data. Therefore, the accuracy index for the estimations, according to different wavelength ranges (whole range, D1 and D2), are shown in Table 3.

In light of the results presented in Fig. 11, a relatively good agreement of the estimation by both methods and the reference track irregularities is observed across the entire length of the scaled track. A very accurate estimation of relative irregularities (gauge variation and cross level) is observed in Fig. 11, by both methods. These good results can be confirmed with the accuracy index presented in Table 3: values of J = 0.18 and 0.31 mm, respectively for the (TRV + TS) method, and J = 0.16 and 0.15 mm, respectively for the (TRV + KF) method.

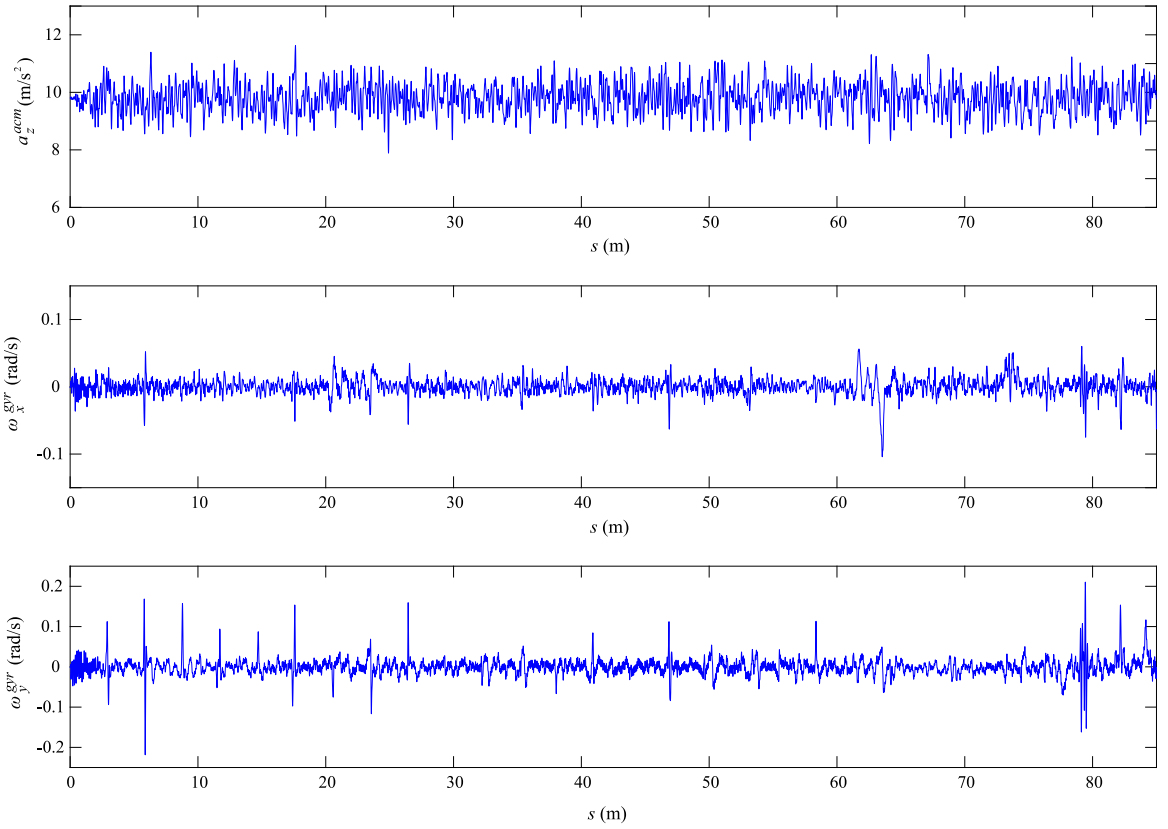

Fig. 10. Sensor data related to vertical motion.

Table 3
Accuracy index, J (in mm) for both methods, in different wavelength ranges.

	TRV + TS method			TRV + KF method		
	D1 + D2	D1 range	D2 range	D1 + D2	D1 range	D2 range
Alignment	1.48	0.87	1.08	2.75	0.42	2.69
Vertical profile	1.21	0.86	0.73	1.51	0.66	1.29
Gauge variation	0.18	0.15	0.09	0.16	0.15	0.05
Cross level	0.31	0.24	0.18	0.15	0.11	0.10

However, the highest disagreement has been encountered in the estimation of global irregularities (lateral alignment and vertical profile), as it can be observed in Fig. 11. The accuracy indices for lateral alignment and vertical profile are 2.75 and 1.51 mm respectively for the proposed method (TRV + KF). These J values are slightly larger than those obtained with the alternative method (TRV + TS). Apparently, such values of accuracy index J may look excessive in the estimation of global irregularities. However, part of these errors is due to the phase delay between the estimated and reference irregularities, along the transition segments (for track lengths around 22, 51, 60 and 75 m), as observed in Fig. 11. This fact can be better observed in the estimation results filtered in the different wavelength ranges: D1 in Fig. 12 and D2 in Fig. 13. Very good results are obtained in the estimation of lateral alignment and vertical profile by the proposed method (TRV + KF) in the D1 range, as it can be observed in Fig. 12 and contrasted in Table 3: J = 0.42 and 0.66 mm, respectively. In fact, these J values are even better than those obtained with the alternative (TRV + TS) method. However, the phase delay in the estimation of these irregularities in the D2 range are clearly observed in Fig. 13, which is reflected in the values of the accuracy index presented in Table 3: J = 2.69 and 1.29 mm, respectively. These poor results in the estimation along the transition segments, especially accused in the D2 range, could be explained by the non-stationary motion of the vehicle along these segments, which make the kinematic model reproduce vehicle motion incorrectly. In order to improve the estimation method proposed in this work, the kinematic model should be redesigned, since there are several assumptions that could not be fulfilled in the transition segments. This will be addressed in a future work.

As a conclusion, the method proposed in this work (TRV + KF) to estimate track irregularities has been validated, obtaining very good results, especially in the short wavelength range (D1), which is the most influential one in dynamic behaviour of the vehicle. In fact, it is common practice in the geometry measurement of metropolitan trains to measure irregularities just in the D1 wavelength

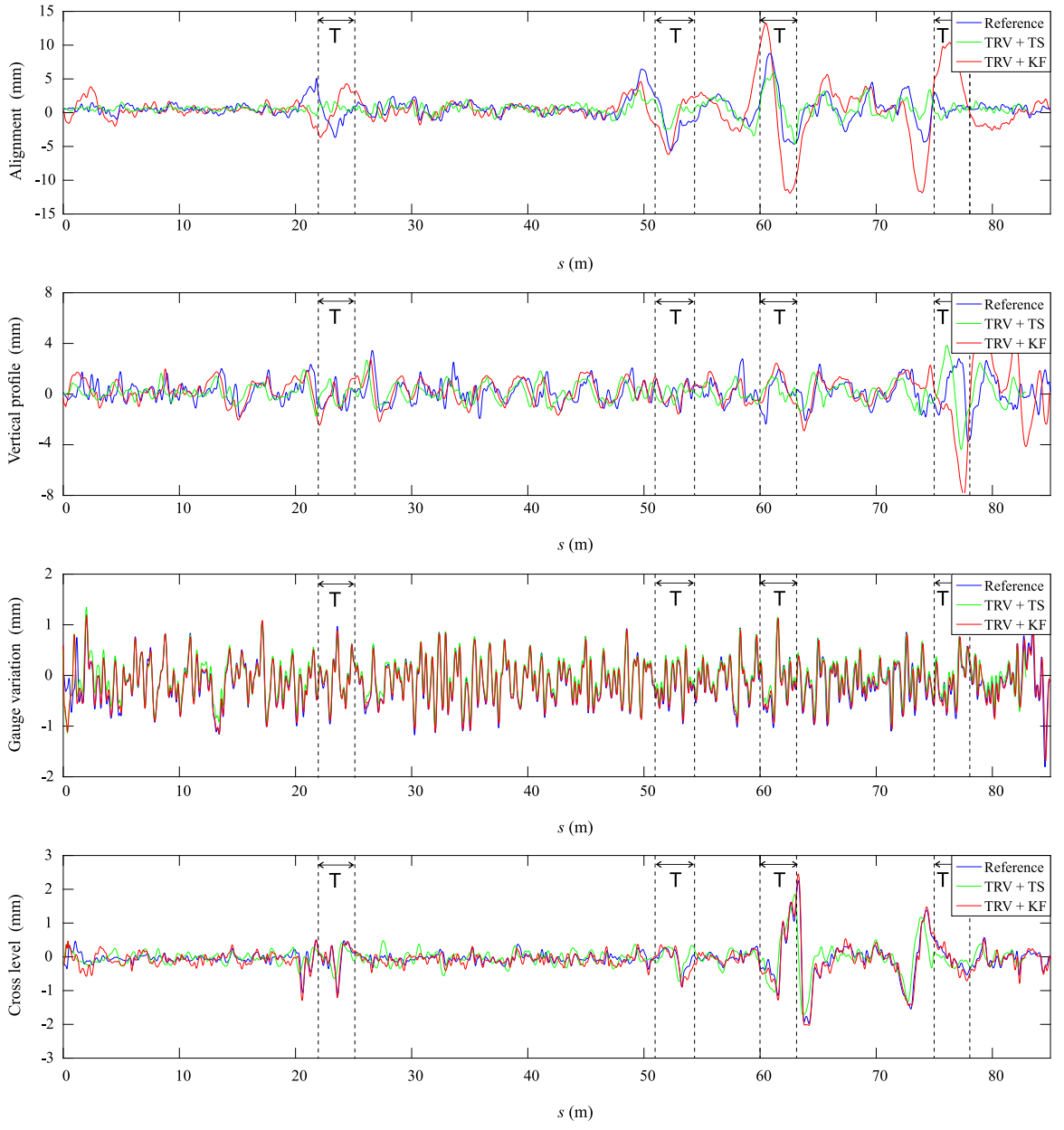

Fig. 11. Track irregularities estimation by both methods under study, filtered in a D1–D2 range (λ = 0.3–7 m).

range. In comparison with the alternative method proposed by the authors (TRV + TS), similar results have been obtained in the estimation of track irregularities. However, the simplicity and speed of measurement make the methodology proposed in the present work especially attractive to be implemented in real tracks, due to the fact that it does not need the use of a total station, which makes the measurement process really tedious and slow.

Finally, in order to test the efficiency of the proposed Kalman filtering method, the computing time to simulate the case under study has been calculated. The algorithm has been developed in Matlab R2016a with a computer with an Intel Core i7 CPU 10875H 2.3 GHz processor. Only 19.7 s of computation time have been required to simulate the total time of the case under study, 123 s, corresponding to 85 m of track length. In this estimation algorithm, the temporal discretization is Δt = 0.004 s, corresponding to the acquisition rate of the sensors (250 Hz). The computational time can even be improved significantly if the Kalman filter is implemented using a low-level programming language like Fortran or C/C++. Consequently, the proposed algorithm is particularly appropriate for real-time applications.

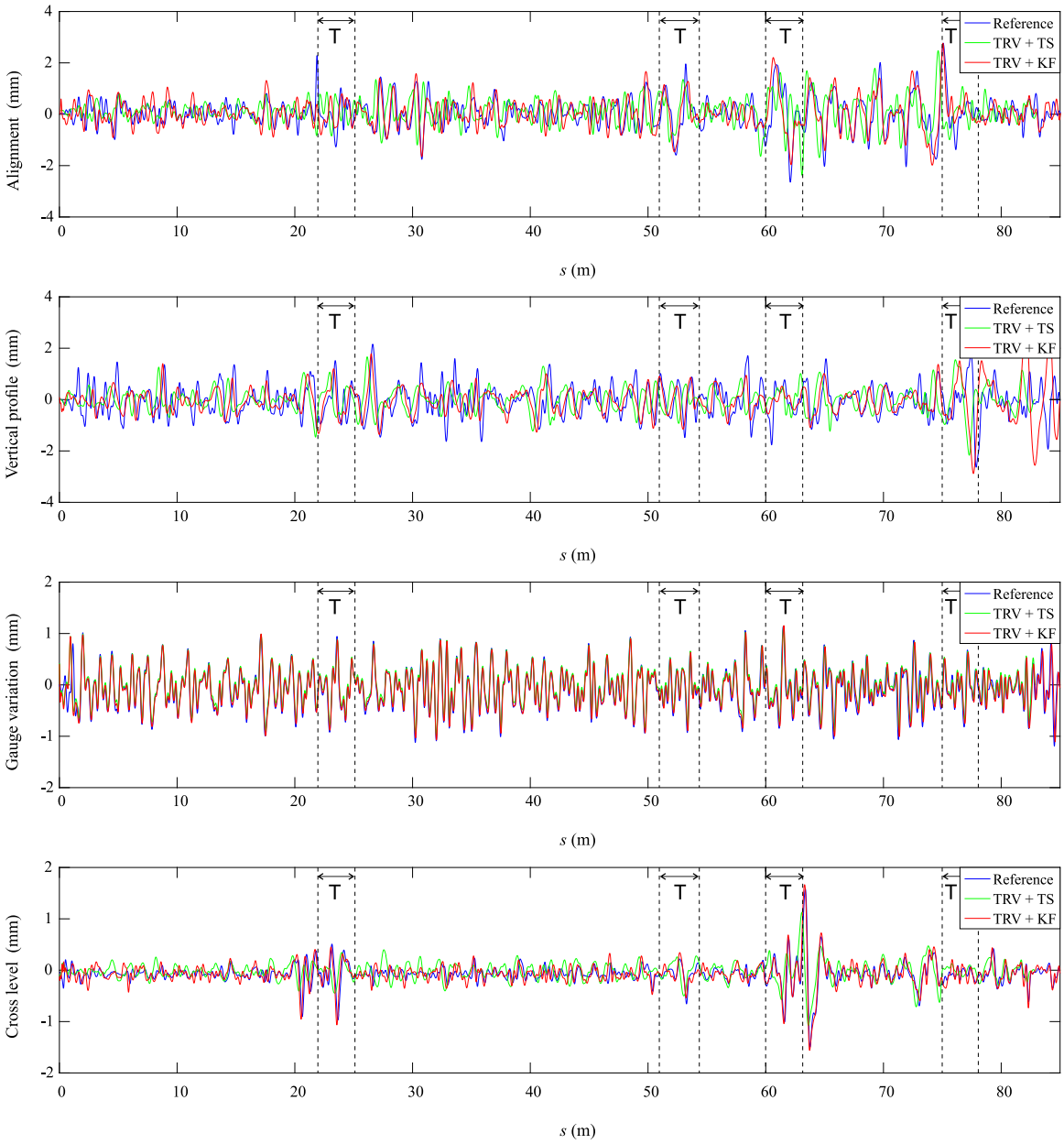

Fig. 12. Track irregularities estimation by both methods under study, filtered in the D1 range (λ = 0.3–2.5 m).

7. Summary and conclusions

In this work, a model-based Kalman filter estimator has been proposed to be used on a Track Recording Vehicle (TRV) for the measurement of track geometry and the estimation of irregularities. The proposed technique is based on the Kalman filtering method, using the measurement from different sensors mounted on a TRV: an Inertial Measurement Unit (IMU), a gauge sensor and a position encoder. This methodology allows a fast and accurate measurement of track irregularities, without the use of a total station (which usually makes the measurement process very slow). The proposed methodology has been experimentally validated on a 1:10 scaled track facility at the University of Seville, comprised of a 90 m long scaled track and an instrumented TRV. The use of the scaled TRV allows the measurement of the 90-metre long scaled track at an operation velocity of V = 0.7 m/s in only two minutes. The results of the estimation of track irregularities have been analysed in the space domain, the different wavelength ranges according to standards. The proposed method (TRV + KF) has also been compared with an alternative methodology previously proposed by the authors (TRV + TS), which also makes use of the TRV, with the addition of a total station.

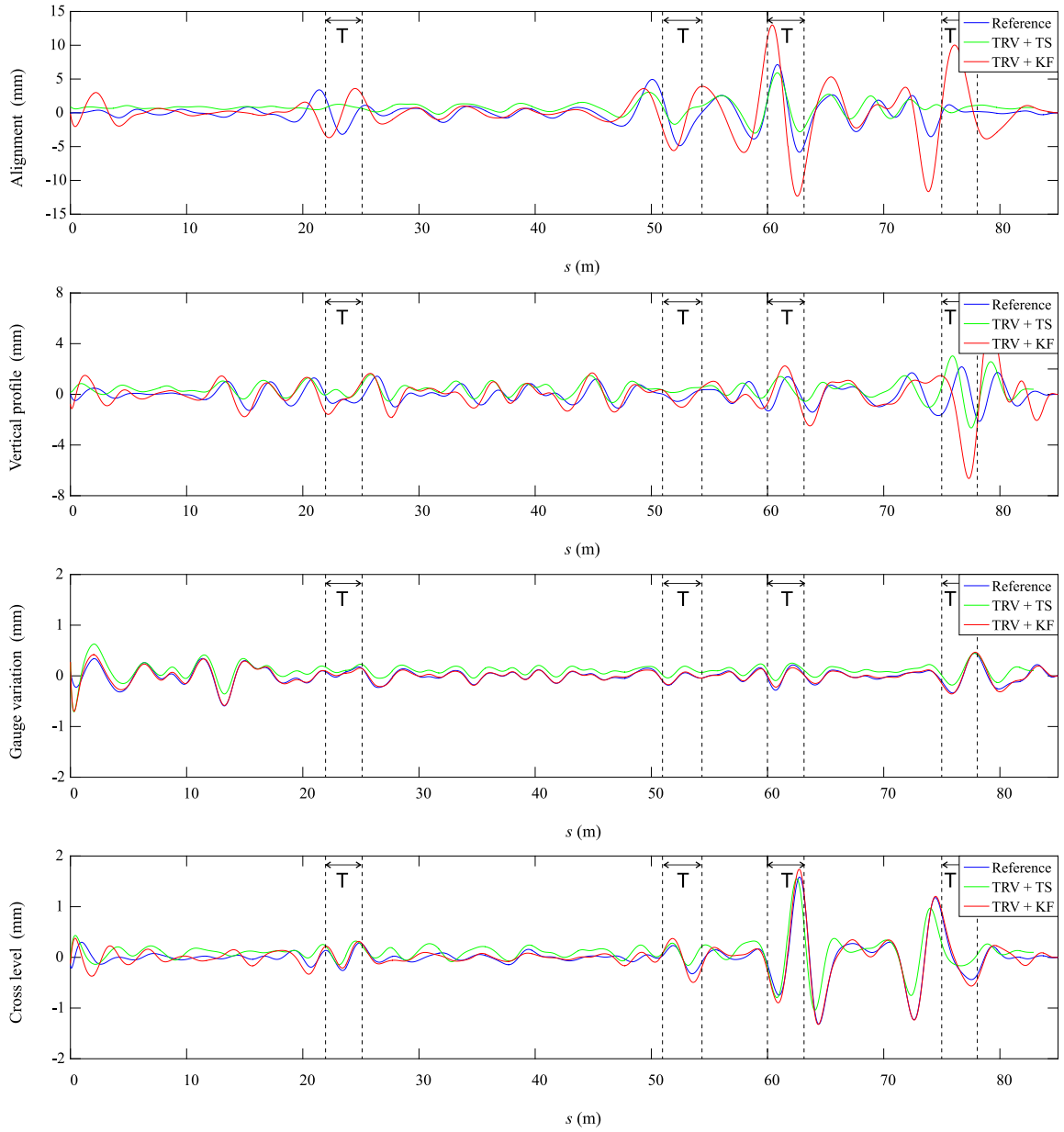

Fig. 13. Track irregularities estimation by both methods under study, filtered in the D2 range (λ = 2.5–7 m).

The results obtained with the proposed method are promising, showing a good performance in measuring track irregularities on straight and curved tracks. A very accurate estimation of relative irregularities (gauge variation and cross level) have been obtained, with errors around 0.15 mm. The highest disagreement was encountered in the estimation of global irregularities (lateral alignment and vertical profile), with errors around 1.5–2.75 mm. However, part of these errors is due to the phase delay between the real and estimated irregularities along the transition segments, especially accused in the long wavelength range (D2), which is less influential on dynamic behaviour of a vehicle. When analysing the short wavelength range (D1), these errors were reduced to around 0.4–0.6 mm. In comparison with the alternative method proposed by the authors (TRV + TS), similar results are obtained in the estimation of track irregularities, but with the advantage of not needing a total station. This makes the proposed methodology very attractive in terms of simplicity and speed in the measurement of track irregularities. Especially promising are the results obtained with the proposed method, when comparing with alternative methods and technologies in literature, which are normally not able to measure all four types of irregularities at the same time, and hardly obtain errors lower than 0.6 mm in the estimation of track irregularities. Additionally, the efficiency of the proposed estimator has been checked, showing a very low computational cost, which makes it especially appropriate for real-time applications.

CRediT authorship contribution statement

Sergio Muñoz: Term, Conceptualization, Methodology, Software, Validation, Writing – review & editing. **Pedro Urda:** Methodology, Validation, Investigation, Resources, Writing – review & editing. **José L. Escalona:** Conceptualization, Methodology, Writing – review & editing, Project administration.

Declaration of competing interest

The authors declare that they have no known competing financial interests or personal relationships that could have appeared to influence the work reported in this paper.

Acknowledgements

This work is supported by *Conserjería de Economía*, Conocimiento, Empresas *y* Universidad de la Junta de Andalucía, under the program "Programa Operativo FEDER 2014–2020", with project reference US-1257665, awarded to the University of Seville, financed with the European Regional Development Fund (FEDER).

References

[1] CEN European Commitee for Standarization, Railway applications - track - track geometry quality - IS EN 13848-5, 2009.
[2] Amberg survey GRP 1000, 2020, https://ambergtechnologies.com/solutions-services/amberg-rail/amberg-survey/ (Accessed: 2020-10-20).
[3] CAT — COrrugation analysis trolley, 2020, https://www.railmeasurement.com/corrugation-analysis-trolley-cat/ (Accessed: 2020-10-20).
[4] Q. Chen, X. Niu, L. Zuo, T. Zhang, F. Xiao, Y. Liu, J. Liu, A railway track geometry measuring trolley system based on aided INS, Sensors 18 (2) (2018) 538, http://dx.doi.org/10.3390/s180205388.
[5] Q. Zhang, Q. Chen, X. Niu, C. Shi, Requirement assessment of the relative spatial accuracy of a motion-constrained GNSS/INS in shortwave track irregularity measurement, Sensors 19 (2019) 5296, http://dx.doi.org/10.3390/s19235296.
[6] A. Sanchez, J.L. Bravo, A. Gonzalez, Estimating the accuracy of track-surveying trolley measurements for railway maintenance planning, J. Surv. Eng. 143 (1) (2017) http://dx.doi.org/10.1061/(ASCE)SU.1943-5428.0000197.
[7] C. Esveld, Modern Railway Track, MRT-productions Zaltbommel, 2006.
[8] P. Weston, C. Roberts, G. Yeo, E. Stewart, Perspectives on railway track geometry condition monitoring from in-service railway vehicles, Veh. Syst. Dyn. 53 (7) (2015) 1063–1091, http://dx.doi.org/10.1080/00423114.2015.1034730.
[9] L. Chia, B. Bhardwaj, P. Lu, R. Bridgelall, Railroad track condition monitoring using inertial sensors and digital signal processing: A review, IEEE Sens. J. 19 (1) (2019) 25–33, http://dx.doi.org/10.1109/JSEN.2018.2875600.
[10] Y. Yang, G. Liu, C. Liu, Fine interrelation between track irregularities and vehicle responses: multi-scale time-dependent correlation analysis, Veh. Syst. Dyn. (2020) 1–19, http://dx.doi.org/10.1080/00423114.2020.1741653.
[11] S. Lei, Y. Ge, Q. Li, Effect and its mechanism of spatial coherence of track irregularity on dynamic responses of railway vehicles, Mech. Syst. Signal Process. 145 (2020) 106957, http://dx.doi.org/10.1016/j.ymssp.2020.106957.
[12] J. Real, P. Salvador Zuriaga, L. Montalbán-Domingo, M. Bueno, Determination of rail vertical profile through inertial methods, Proc. Inst. Mech. Eng. F-J. Rail Rapid Transit - Proc. Inst. Mech. Eng. F-J. Rail. R 1 (2010) 1–10, http://dx.doi.org/10.1243/09544097JRRT353.
[13] A. De Rosa, S. Alfi, S. Bruni, Estimation of lateral and cross alignment in a railway track based on vehicle dynamics measurements, Mech. Syst. Signal Process. 116 (2019) 606–623, http://dx.doi.org/10.1016/j.ymssp.2018.06.041.
[14] S. Kraft, J. Causse, A. Martinez, Black-box modelling of nonlinear railway vehicle dynamics for track geometry assessment using neural networks, Veh. Syst. Dyn. 57 (9) (2019) 1241–1270, http://dx.doi.org/10.1080/00423114.2018.1497186.
[15] A.D. Rosa, R. Kulkarni, A. Qazizadeh, M. Berg, E.D. Gialleonardo, A. Facchinetti, S. Bruni, Monitoring of lateral and cross level track geometry irregularities through onboard vehicle dynamics measurements using machine learning classification algorithms, Proc. Inst. Mech. Eng. F: J. Rail Rapid Transit, 0 (0) (0) 0954409720906649, http://dx.doi.org/10.1177/0954409720906649.
[16] H. Tsunashima, Condition monitoring of railway tracks from car-body vibration using a machine learning technique, Appl. Sci. 9 (2019) 2734, http://dx.doi.org/10.3390/app9132734.
[17] M. Jesussek, K. Ellermann, Fault detection and isolation for a full-scale railway vehicle suspension with multiple Kalman filters, Veh. Syst. Dyn. 52 (12) (2014) 1695–1715, http://dx.doi.org/10.1080/00423114.2014.959026.
[18] M. Jesussek, K. Ellermann, Fault detection and isolation for a nonlinear railway vehicle suspension with a hybrid extended Kalman filter, Veh. Syst. Dyn. 51 (10) (2013) 1489–1501, http://dx.doi.org/10.1080/00423114.2013.810764.
[19] A. Onat, P. Voltr, M. Lata, An unscented Kalman filter-based rolling radius estimation methodology for railway vehicles with traction, Proc. Inst. Mech. Eng. F: J. Rail Rapid Transit 232 (6) (2018) 1686–1702, http://dx.doi.org/10.1177/0954409717745201.
[20] Y. Zhao, B. Liang, S. Iwnicki, Friction coefficient estimation using an unscented Kalman filter, Veh. Syst. Dyn. 52 (sup1) (2014) 220–234, http://dx.doi.org/10.1080/00423114.2014.891757.
[21] M. Odashima, S. Azami, Y. Naganuma, H. Mori, H. Tsunashima, Track geometry estimation of a conventional railway from car-body acceleration measurement, Mech. Eng. J. 4 (1) (2017) 16–00498–16–00498, http://dx.doi.org/10.1299/mej.16-00498.
[22] J. Seok Lee, S. Choi, S.-S. Kim, C. Park, Y. Guk Kim, A mixed filtering approach for track condition monitoring using accelerometers on the axle box and bogie, IEEE Trans. Instrum. Meas. 61 (2012) 749–758.
[23] X. Wei, F. Liu, L. Jia, Urban rail track condition monitoring based on in-service vehicle acceleration measurements, Measurement 80 (2016) 217–228, http://dx.doi.org/10.1016/j.measurement.2015.11.033.
[24] X. Xiao, Z. Sun, W. Shen, A Kalman filter algorithm for identifying track irregularities of railway bridges using vehicle dynamic responses, Mech. Syst. Signal Process. 138 (2020) 106582, http://dx.doi.org/10.1016/j.ymssp.2019.106582.
[25] A.S. Lathe, A. Gautam, Estimating vertical profile irregularities from vehicle dynamics measurements, IEEE Sens. J. 20 (1) (2020) 377–385, http://dx.doi.org/10.1109/JSEN.2019.2942317.
[26] Q. Jiang, W. Wu, Y. Li, M. Jiang, Millimeter scale track irregularity surveying based on ZUPT-aided ins with sub-decimeter scale landmarks, Sensors 17 (2017) 2083, http://dx.doi.org/10.3390/s17092083.
[27] Z. Gao, M. Ge, Y. Li, W. Shen, H. Zhang, H. Schuh, Railway irregularity measuring using rauch-tung-striebel smoothed multi-sensors fusion system: quad-GNSS PPP, IMU, odometer and track gauge, GPS Solut. 22 (2018) 36, http://dx.doi.org/10.1007/s10291-018-0702-5.

[28] P.F. Weston, C.S. Ling, C.J. Goodman, C. Roberts, P. Li, R.M. Goodall, Monitoring lateral track irregularity from in-service railway vehicles, Proc. Inst. Mech. Eng. F: J. Rail Rapid Transit 221 (1) (2007) 89–100, http://dx.doi.org/10.1243/0954409JRRT64.
[29] J.L. Escalona, P. Urda, S. Muñoz, A track geometry measuring system based on multibody kinematics, inertial sensors and computer vision, Sensors 21 (3) (2021) http://dx.doi.org/10.3390/s21030683.
[30] G. Welch, G. Bishop, An introduction to the kalman filter, 2006.
[31] S. Muñoz, J. Ros, P. Urda, J.L. Escalona, Estimation of lateral track irregularity using a Kalman filter. experimental validation, J. Sound Vib. 504 (2021) 116122, http://dx.doi.org/10.1016/j.jsv.2021.116122.
[32] P. Urda, J.F. Aceituno, S. Muñoz, J.L. Escalona, Measurement of railroad track irregularities using an automated recording vehicle, Measurement 183 (2021) 109765, http://dx.doi.org/10.1016/j.measurement.2021.109765.